ISSN (Print) : 0974-6846
ISSN (Online) : 0974-5645
Indian Journal of Science and Technology, *Vol 10(31), DOI: 10.17485/ijst/2017/v10i31/114486, August 2017*

Studies on Molecular Structure and Vibrational Spectra of NLO Crystal L-Glutamine Oxalate by DFT Method

G. Edwin Sheela[1,3], D. Manimaran[2], I. Hubert Joe[2]* and V. Bena Jothy[3]

[1]Department of Physics, Muslim Arts College, Thiruvithancode - 629174, Tamil Nadu, India; sheelalivings@gmail.com
[2]Centre for Molecular and Biophysics Research, Department of Physics, Mar Ivanios College, Thiruvananthapuram - 695015, Kerala, India; hubertjoe@gmail.com
[3]Department of Physics, Women's Christian College, Nagercoil - 629001, Tamil Nadu, India; benaezhil@yahoo.com

Abstract

Objectives: To explicate structural features of L-GLUTAMINE OXALATE (LGO) using vibrational spectroscopic methods and DFT computations. To identify the functional groups and hydrogen bonding interactions of the molecule by recording FTIR and FT-Raman spectra. To confirm NLO activity by performing SHG test. **Methods/Statistical Analysis:** Crystals were grown by slow evaporation method and characterized by powder X-Ray diffraction method. FTIR, FT-Raman, UV-Vis analysis and second harmonic generation test were predicted. DFT analysis using Gaussian'09 program package were performed to confirm the NLO properties theoretically. **Findings**: Lowering of HOMO-LUMO energy gap value explains the intramolecular charge-transfer interaction which indicates NLO property. Second Harmonic Generation of the sample shows good nonlinearity of the sample. **Application/Improvements:** LGO sample shows good NLO Properties and can be used in optical field.

Keywords: HOMO-LUMO, MEP, NLO, NCA

1. Introduction

Nonlinear optical materials find wide applications in laser and data storage technology[1,2]. Amino acids exhibit nonlinear optical (NLO) properties. L-Glutamine is an amino acid which finds in the human body in large quantity. The major function of this amino acid is to relocate nitrogen to the body and regulates the amount of nitrogen present in the body. It keeps the required nitrogen within the body and provides proper growth and development of muscles.

Compounds of amino acids with inorganic oxyacids are important materials for photonic applications. Study of L-Glutamine[3] has been reported earlier. The structural, thermal and optical properties of bis L-glutamine sodium nitrate have been studied by Hanumantharao et al[4]. Qiushuo Yu et al[5] reported the solubility, dissolution enthalpy and entropy of L-glutamine in mixed solvents of ethanol + water and acetone + water. The charge transfer interaction, vibrational spectra and DFT computation of L-Glutamine Picrate were reported by Amalanathan

*Author for correspondence

et al[6]. The present work deals with a detailed vibrational spectral analysis of new NLO crystal L-Glutamine oxalate (LGO) using normal coordinate analysis (NCA). Natural bond orbital (NBO) analysis, HOMO-LUMO energy gap analysis and NLO effects using Gaussian'09 program were also predicted.

2. Experimental Details

L-Glutamine and oxalic acid were taken in 1:1 equimolar ratio and dissolved in distilled water, then allowed to evaporate slowly at room temperature. L-Glutamine oxalate crystals were obtained within two weeks. Repeated recrystallization yielded good quality crystals. The X-ray powder diffraction (XPRD) measurements were carried out using a Rigaku powder diffractometer. FTIR and FT-Raman spectra of LGO were recorded. The electronic absorption spectrum using Perkin Elmer Lambda 35 UV-Vis spectrophotometer was recorded in the region 800-200 nm.

3. Theoretical methodology

Molecular structure of LGO was fully optimized using DFT method with B3LYP/6-311++G(d,p) basis set[7-9] as implemented in Gaussian'09 software package[10]. Charge transfer between atoms provide the evidence for inter and intramolecular hydrogen bondings of the molecule and it was analyzed using NBO analysis[11]. NCA has been performed using MOLVIB program version 7.0 written by Sundius[12,13].

4. Results and Discussion

4.1 X-ray Powder Diffraction Analysis

Bragg peaks are observed at specific 2θ angles. The 'd'spacings and (h k l) values for prominent peaks are identified. XRD peaks at 2θ have been indexed using CRYSFIRE software. The theoretical hkl values were derived from experimental diffraction pattern. Indexed

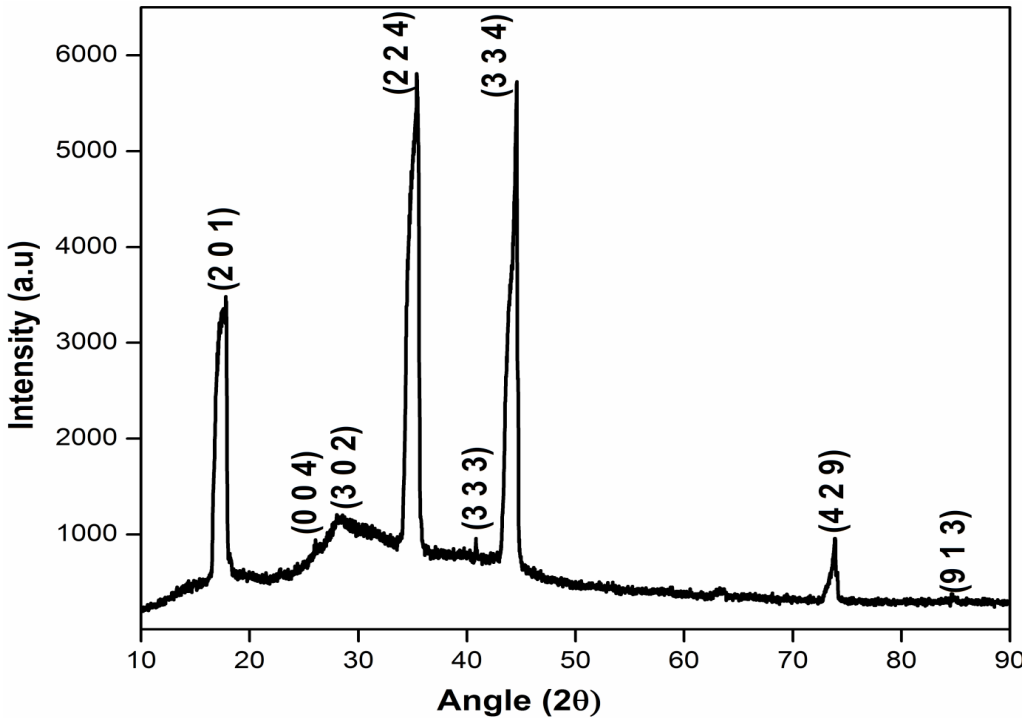

Figure 1. X-ray diffraction pattern of LGO.

Table 1. Powder X-ray Diffraction data of LGO

Unit Cell Parameters			2 Observed	2 Calculated	'd' Observed
h	k	l			
2	0	1	17.790	17.776	4.9818
0	0	4	26.070	26.080	3.4153
3	0	2	28.180	28.183	3.1642
2	2	4	35.380	35.370	2.5350
3	3	3	40.840	40.841	2.2078
3	3	4	44.600	44.604	2.0300
4	2	9	73.880	73.880	1.2817
9	1	3	84.610	84.578	1.1444

PXRD pattern and data have been presented in Figure 1 and Table 1. The appearance of sharp peaks confirmed the crystallinity nature of the grown sample. The estimated lattice parameters were comparable with the data available in JCPDS standards (file numbers: 39-1835, 20-1816 and 20-1817). The unit cell parameters which are calculated for LGO are a=b=10.710Å, c=13.655Å, α=β=γ=90°. These values confirm the title compound is in tetragonal crystal system.

4.2 Optimized Geometry Analysis

Molecular structure with atom numbering scheme of LGO is shown in Figure 2. The optimized structural parameters are tabulated in Table 2. The calculated bond lengths of N_{15}-H_{16}, N_{15}-H_{17} and N_{15}-H_{28} are found to be 1.0313, 1.0233 and 1.1137Å, respectively. Elongation of bond length N_{15}-H_{28} (1.1137Å) reveals the possibility of N-H···O hydrogen bonding. Bond length of O_{21}···H_{28}

(1.4735Å), is less than the vander Waals radii of O and H atoms, shows the presence of N-H···O hydrogen bonding. The bond angle N_{15}-H_{28}···O_{21}(170.3266°) is within the angle limit and interaction path is linear which indicates the intramolecular charge transfer interaction. The calculated bond lengths of N_6-H_7, N_6-H_8 are found to be 1.0105 and 1.01603Å, respectively. Elongation of N_6-H_8 shows the possibility of N-H···O hydrogen bonding. The bond length O_{25}···H_8 (2.1389Å) is less than the vander Waals radii of O and H atoms, shows the presence of N_6-H_8···O_{25} hydrogen bonding.

4.3 Natural Bond Orbital Analysis

The natural bond orbitals were analyzed using NBO 3.1 program at DFT/B3LYP level. The second-order Fock matrix was carried out to evaluate the donor-acceptor interactions in the NBO basis[15] which is presented in Table 3. $LPO_{21} \rightarrow \pi^*(C_{22}$-$O_{23})$ interaction gives the strongest stabilization to the system by 86.99 kcal/mol. The increasing interaction energy is due to the strong delocalization leading to stabilization of the molecule. Orbital overlap between bonding $\sigma(N_{15}$-$H_{28})$ and antibonding

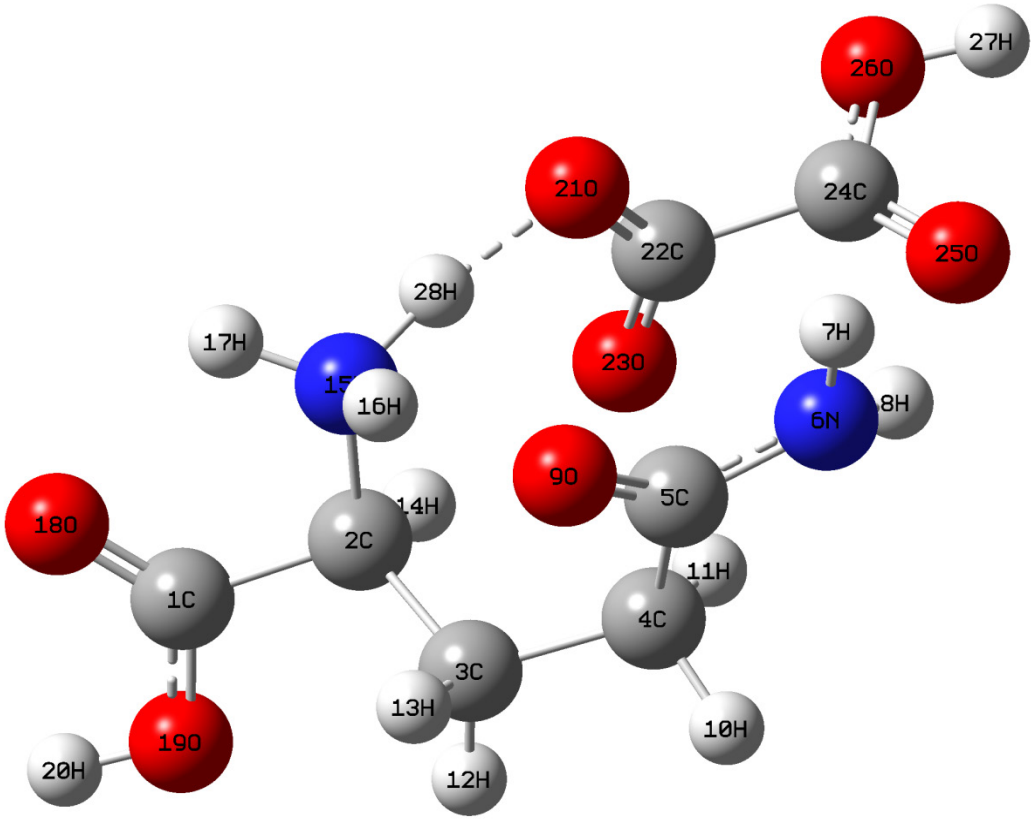

Figure 2. Molecular structure of LGO.

Table 2. Optimized geometrical parameters of LGO

Bond length	Cal. (Å)	Bond angle	Cal. (°)	Dihedral angle	Cal. (°)
C_1-C_2	1.5194	C_2-C_1-O_{18}	124.0579	O_{18}-C_1-C_2-C_3	129.3512
C_1-O_{18}	1.2083	C_2-C_1-O_{19}	112.254	O_{18}-C_1-C_2-H_{14}	-110.1362
C_1-O_{19}	1.3409	O_{18}-C_1-O_{19}	123.6659	O_{18}-C_1-C_2-N_{15}	4.0874
C_2-C_3	1.5405	C_1-C_2-C_3	113.2618	O_{19}-C_1-C_2-C_3	-52.3092
C_2-H_{14}	1.0987	C_1-C_2-H_{14}	107.7692	O_{19}-C_1-C_2-H_{14}	68.2033
C_2-N_{15}	1.4982	C_1-C_2-N_{15}	107.6586	O_{19}-C_1-C_2-N_{15}	-177.573
C_3-C_4	1.535	C_3-C_2-H_{14}	108.8852	C_2-C_1-O_{19}-H_{20}	-177.4056
C_3-H_{12}	1.0908	C_3-C_2-N_{15}	112.682	O_{18}-C_1-O_{19}-H_{20}	0.9416
C_3-H_{13}	1.0938	H_{14}-C_2-N_{15}	106.2446	C_1-C_2-C_3-C_4	176.5652
C_4-C_5	1.5285	C_2-C_3-C_4	114.6094	C_1-C_2-C_3-H_{12}	56.2315
C_4-H_{10}	1.0955	C_2-C_3-H_{12}	106.6507	C_1-C_2-C_3-H_{13}	-59.824
C_4-H_{11}	1.093	C_2-C_3-H_{13}	109.7376	H_{14}-C_2-C_3-C_4	56.6879
C_5-N_6	1.3501	C_4-C_3-H_{12}	108.6984	H_{14}-C_2-C_3-H_{12}	-63.6457

Table 2 Continued

C_5-O_9	1.234	C_4-C_3-H_{13}	109.4551	H_{14}-C_2-C_3-H_{13}	-179.7013
N_6-H_7	1.0106	H_{12}-C_3-H_{13}	107.4176	N_{15}-C_2-C_3-C_4	-60.9194
N_6-H_8	1.016	C_3-C_4-C_5	113.7999	N_{15}-C_2-C_3-H_{12}	178.7469
N_{15}-H_{16}	1.0313	C_3-C_4-H_{10}	108.3871	N_{15}-C_2-C_3-H_{13}	62.6914
N_{15}-H_{17}	1.0233	C_3-C_4-H_{11}	110.9735	C_1-C_2-N_{15}-H_{16}	107.0045
N_{15}-H_{28}	1.1137	C_5-C_4-H_{10}	106.2053	C_1-C_2-N_{15}-H_{17}	-13.6424
O_{19}-H_{20}	0.9698	C_5-C_4-H_{11}	110.7316	C_1-C_2-N_{15}-H_{28}	-135.3717
O_{21}-C_{22}	1.2689	H_{10}-C_4-H_{11}	106.3261	C_3-C_2-N_{15}-H_{16}	-18.6047
O_{21}-H_{28}	1.4735	C_2-N_{15}-H_{16}	110.3271	C_3-C_2-N_{15}-H_{17}	-139.2516
C_{22}-O_{23}	1.2355	C_2-N_{15}-H_{17}	109.1016	C_3-C_2-N_{15}-H_{28}	99.0191
C_{22}-C_{24}	1.5349	C_2-N_{15}-H_{28}	109.3834	H_{14}-C_2-N_{15}-H_{16}	-137.7593
C_{24}-O_{25}	1.2146	H_{16}-N_{15}-H_{17}	109.7554	H_{14}-C_2-N_{15}-H_{17}	101.5937
C_{24}-O_{26}	1.3393	H_{16}-N_{15}-H_{28}	107.1487	C_4-C_5-N_6-H_7	174.2297
O_{26}-H_{27}	0.9712	H_{17}-N_{15}-H_{28}	111.1109	H_{13}-C_3-C_4-H_{11}	-174.3552

Table 3. Second-order perturbation theory analysis of Fock matrix in NBO basis for LGO

Donor NBO (i)	E(D)	Acceptor NBO(j)	E(D)	E(2)[a]kcal/mol	E(j)-E(i)[b] a.u.	F(i,j)[c] a.u.
LP (1) N_6	1.7176	$\sigma^*(C_5 - O_9)$	0.0340	2.65	0.83	0.045
LP (1) N_6	1.7176	$\pi^*(C_5 - O_9)$	0.2967	48.77	0.31	0.110
LP (1) O_9	1.9755	$\sigma^*(C_4-C_5)$	0.0641	2.62	1.06	0.048
$\sigma(N_{15} - H_{28})$	1.9864	$\sigma^*(O_{21}-C_{22})$	0.0617	0.32	1.17	0.017
LP(1) O_{21}	1.9561	$\sigma^*(N_{15}-H_{28})$	0.1423	10.88	0.91	0.091
LP(2) O_{21}	1.8069	$\sigma^*(N_{15}-H_{28})$	0.1423	54.07	0.65	0.169
LP(3)O_{21}	1.8069	$\sigma^*(N_{15}-H_{28})$	0.1423	8.22	0.56	0.064
LP(3)O_{21}	1.8069	$\pi^*(C_{22}-O_{23})$	0.3384	86.99	0.28	0.140
LP(2)O_{26}	1.8090	$\pi^*(C_{24} -O_{25})$	0.2137	40.22	0.39	0.112
LP(2)O_{23}	1.8508	$\sigma^*(O_{21}-C_{22})$	0.0617	19.12	0.78	0.111
LP(2)O_{23}	1.8508	$\sigma^*(C_{22}-C_{24})$	0.1250	20.86	0.60	0.100
LP(2)O_{25}	1.8482	$\sigma^*(C_{22}-C_{24})$	0.1250	17.69	0.63	0.095

Table 3 Continued

$LP(2)O_{25}$	1.8482	$\sigma^*(C_{24}\text{-}O_{26})$	0.0895	29.70	0.64	0.125
$LP(1)O_{26}$	1.9755	$\sigma^*(C_{24}\text{-}O_{25})$	0.0356	6.75	1.20	0.080
$LP(2)O_{23}$	1.8508	$\sigma^*(C_{2}\text{-}H_{14})$	0.0315	2.78	0.64	0.039
$LP(2)O_{25}$	1.8482	$\sigma^*(N_{6}\text{-}H_{8})$	0.0199	3.02	0.71	0.043

[a]*Energy of hyperconjugative interactions*

[b]*Energy difference between donor and acceptor*

[c]*Fock matrix element between i and j NBO orbitals*

$\sigma^*(O_{21}\text{-}C_{22})$ results giving stabilization with increase in electron density of the system. The high electron density leads the increase in $N_{15}\text{-}H_{28}$ bond length and decreasing its stretching wavenumber and well explains the red-shift. This charge transfer interaction between $\sigma(N_{15}\text{-}H_{28})\rightarrow\sigma^*(O_{21}\text{-}C_{22})$ supports the existence of N-H···O hydrogen bonding.

4.4 Vibrational Spectral Analysis

The vibrational band assignments have been performed using normal coordinate analysis. According to Pulay's recommendations[16,17] internal coordinates of LGO have been selected. The observed peaks are shown in Table 4 along with detailed assignments. The FTIR and FT-Raman

Table 4. Vibrational assignments of LGO by normal coordinate analysis

Scaled wavenumber (cm^{-1})	Observed fundamentals (cm^{-1})		Assignments with PED(≥10%)
	IR	Raman	
3434	3442w	-	OH str (100)

Table 4 Continued

3406	-	3398w	OH str (100)
3356	-	3336w	NH_2asy.str (86), NH_2sym.str (14)
3212	-	3233w	NH_2sym.str (84), NH_2asy.str (15)
3178	3167s	-	$NH_3^+{}_{ops}$asy.str (49), $NH_3^+{}_{ips}$asy.str (27)
3002	-	3010s	$NH_3^+{}_{ips}$asy.str (56), NH_3^+sym.str (41)
2973	2983s	2983s	CH_2-I asy.str(85), CH_2-I sym.str (11)
2952	2954vs	2934vs	CH_2-IIasy.str(82), CH_2-II sym.str (11)
2917	2917vs	-	CH_2-I sym.str(80), CH_2-I asy.str(13)
2865	2853s	2832w	CHstr(97)
1715	-	1718w	COdbstr (33)
1616	1615vs	1618vw	NH_2sciss (49)
1519	1516vs	-	CH_2-Isciss(61)
1474	-	1474w	CH_2-IIsciss(15)
1433	1444s	-	CH_{op}rock (24), CHrock(11)

Table 4 Continued

1416	1413m	-	NCstr (22), CH_2-II wag(13)
1372	-	1380vw	CH_2-Iwag(49)
1345	1353s	1351vw	CH_2-I twist(17)
1331	1324s	-	CH_2-Iwag (21)
1281	1273m	1260vw	CH_2-IIwag (23), CH_2-I twist(11)
1219	1244m	-	CH_2-II twist (27)
1188	1172m	-	OHbend (29), COstr(28)
1147	1150m	1152vw	CH_2-IItwist(22), NH_3^+rock(10)
1132	1115w	1109vw	NH_2rock(31)
1073	1075w	-	CNstr(37), CCstr(10)
1036	1030w	1040vw	CH_2-IIrock(24)
970	976m	968vw	CCstr(44)
928	920w	922vw	CH_2-Irock(29)
859	870m	875w	CCstr(22)
827	-	832vw	COsym.def.(38), CCstr (16)

Table 4 Continued

809	805w	-	COwag(28), Tor1(27)
760	747w	741w	CCstr(29), CH_2rock(12)
722	721w	715w	COsym.def.(24), CCstr(10)
702	707w	-	COsym.def(45)
676	668w	-	COdbwag (24), NH_2wag(15)
642	645w	-	COtor(14)
608	605w	-	COtor (79)
563	546s	-	COtor(23), NH_3^+tor(15)
519	-	522w	NH_3^+tor(14)
439	453w	-	HOstr (12)
301	-	332w	HO str(23), CCCsciss (12)
242	-	231w	CH_2tor (13), CHtor(16)
166	-	169w	CHtor (24), NH_3^+tor (17)

vs-very strong; s-strong; m-medium; w-weak; str-stretching; bend-bending; ops-out-of-plane stretching; ips-in-planestretching; sym.str-symmetric stretching; asy.str-asymmetric stretching; asy.def-asymmetric deformation; asy.defo-out-of-plane asym.deformation; sym.def-symmetric deformation; wag-wagging; rock-rocking; tor-torsion; sciss-scissoring;

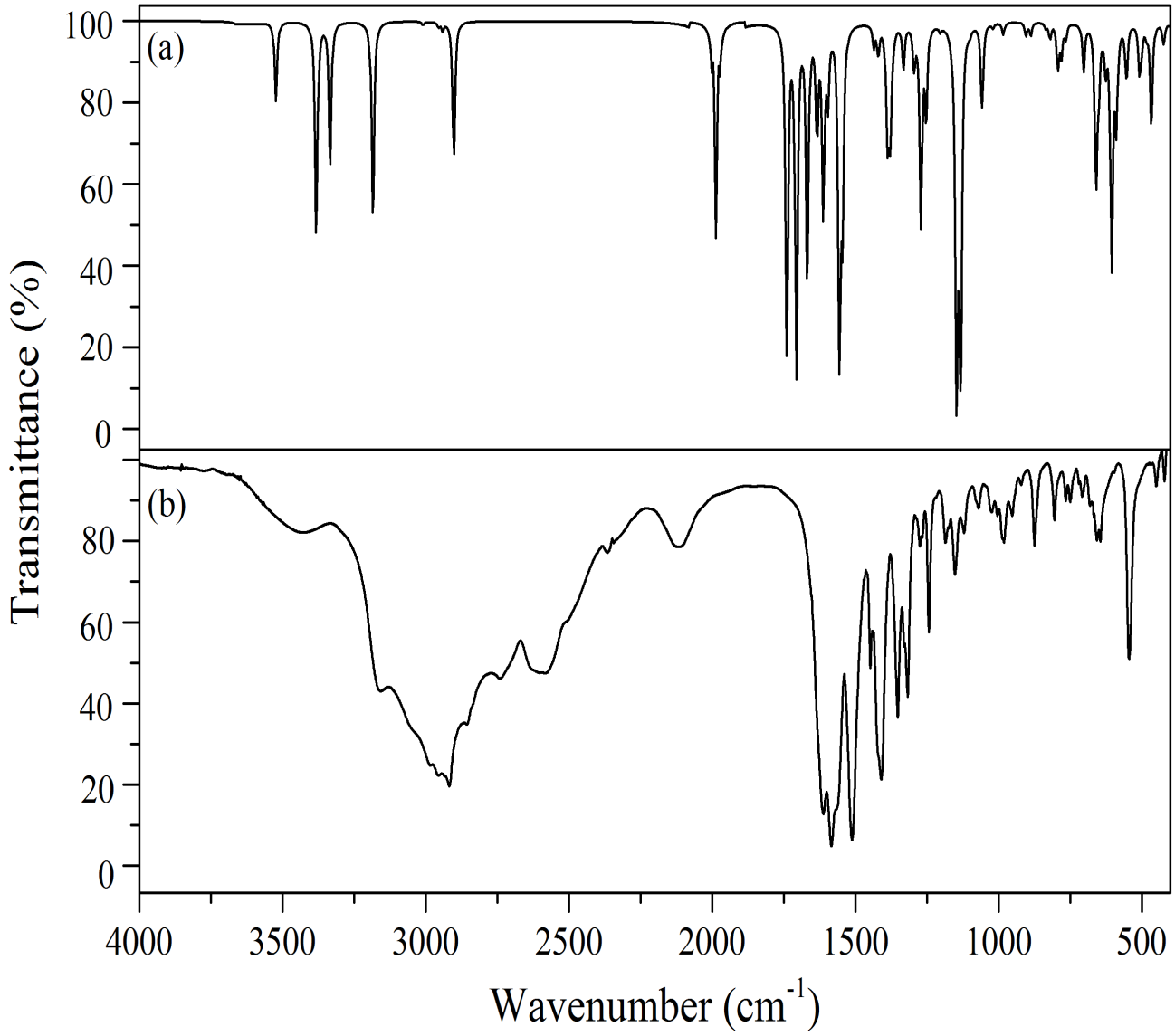

Figure 3. (a) Simulated (b) Experimental FTIR spectra of LGO.

spectra (observed) and theoretical spectra (simulated) are shown in Figures 3 and 4, respectively. Vibrational wavenumbers for various functional groups are discussed below in detail.

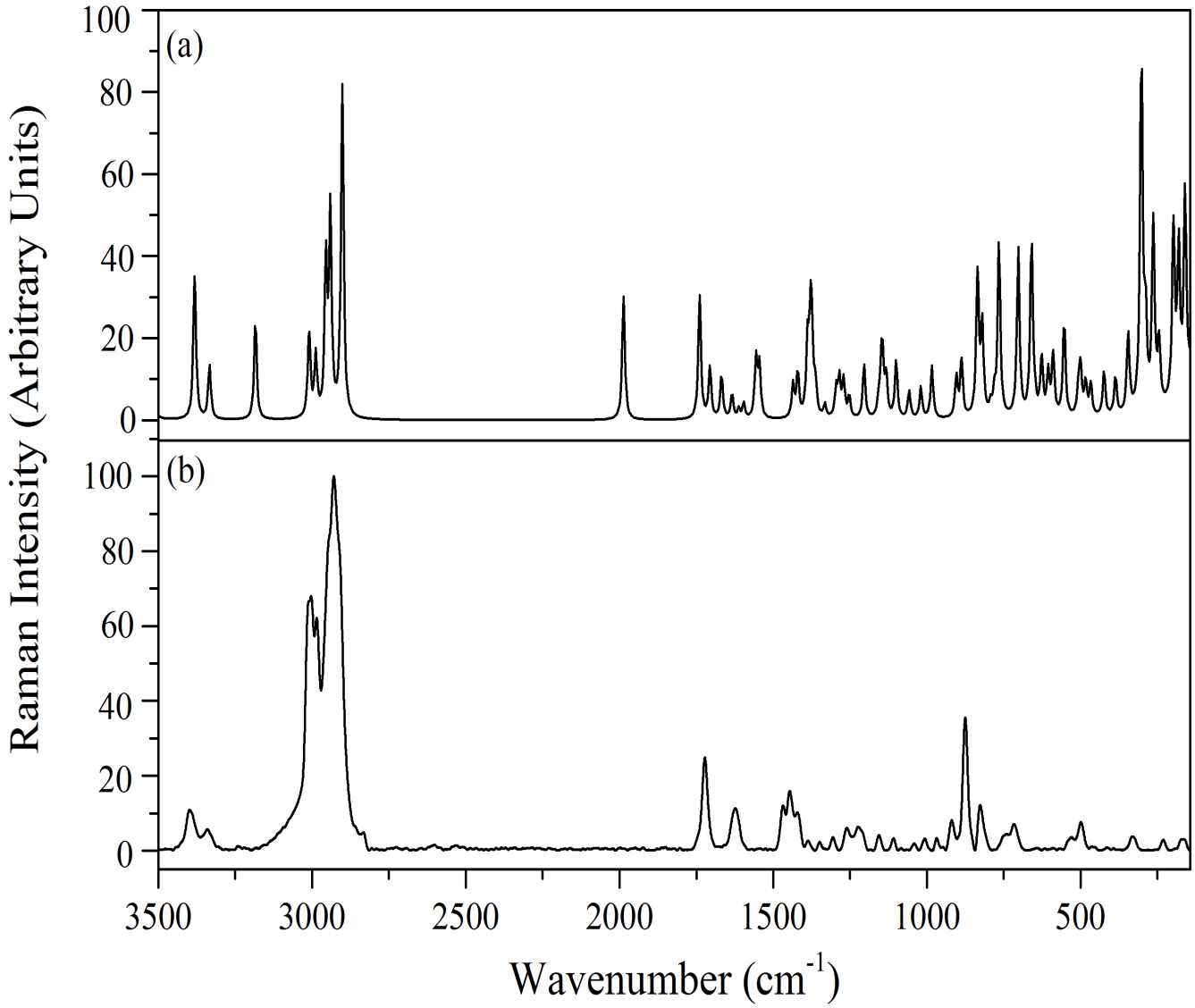

Figure 4. (a) Simulated (b) Experimental FT-Raman spectra of LGO.

4.4.1 OH Vibrations

The broad and strong bands are identified by Hydrogen bondings. The hydroxyl stretching vibrations are generally occur in the region around 3500 cm^{-1}[18,19]. The observed broad IR band at 3442 cm^{-1} and Raman band at 3398 cm^{-1} are assigned to OH stretching modes. Red-shifting of OH stretching wavenumber gives clear evidence for the inter-molecular O-H···O hydrogen bonding in the molecule.

The scaled values (3434, 3406 cm^{-1}) of these modes are in well agreed with the experimental values. The broadening of OH stretching wave number denotes the formation of intermolecular O-H···O hydrogen bonding in solid phase.

4.4.2 NH_2 Vibrations

Asymmetric and symmetric NH_2 stretching vibrations are expected to occur in the region 3380-3350 and 3310-3280 cm^{-1}, respectively[20]. For asymmetric and symmetric stretching modes, the protonation of the NH_2 group can shift the band position in the range 3300-3100 and 3100-2600 cm^{-1}. The asymmetric stretching mode of NH_2 is observed in Raman at 3336 cm^{-1}. The band at 3233 cm^{-1} in Raman is attributed to symmetric stretching mode of NH_2. The wavenumber of the amino group appear at around 1700-1600 cm^{-1} for the scissoring and 1150-900 cm^{-1} for the rocking deformations[18]. The position of absorption in this region depends upon the degree of hydrogen bonding and hence upon physical state of the sample. NH_2 scissoring modes are observed as very strong band at 1615cm^{-1} in IR and as weak band at 1618 cm^{-1} in Raman. The scaled value(1616 cm^{-1}) is in good agreement with the experimental values. NH_2 rocking modes are observed at 1115 cm^{-1} in IR and at 1109 cm^{-1} in Raman.

4.4.3 NH_3+ Vibrations

NH_3^+ asymmetric bands are predicted to occur at 3330 cm^{-1} [21]. The observed strong bands at 3167cm^{-1} in IR and 3010 cm^{-1} in Raman are assigned to asymmetric stretching modes. The scaled value (3178, 3002cm^{-1}) of this modes are in good agreement with the experimental values. The red-shifting of NH_3^+ stretching vibrations indicate the presence of N-H···O hydrogen bonding. The intramolecular hydrogen bonding is responsible for the high β value, and this mechanism plays an important role in the NLO property. NH_3^+ rocking modes are expected to occur around 1000 cm^{-1}[1,22,23]. The bands observed at 1150 cm^{-1} in IR and at 1152 in Raman are assigned to NH_3^+ rocking mode. The scaled value (1147cm^{-1}) of this mode shows excellent agreement with the experimental value.

4.4.4 CH_2 Vibrations

CH_2 asymmetric and symmetric stretching modes normally occur at 2935 cm^{-1} and 2865 cm^{-1}, respectively[24]. Strong band at 2983 cm^{-1} in IR is assigned to CH_2-I asymmetric stretching mode. The Raman counterpart is observed at the same wavenumber with strong intensity. The simultaneous occurrence of CH_2 stretching mode appears in IR and Raman provides evidences for the charge transfer interactions[25,26]. Very strong bands at 2954 cm^{-1} in IR and at 2934 cm^{-1} in Raman are attributed to CH_2-II asymmetric stretching mode. Very intense band at 2917 cm^{-1} in IR is identified to the CH_2-I symmetric stretching mode. The scaled value (2917 cm^{-1}) is in good agreement with the experimental value. Blue-shift of CH_2 stretching wave number indicates the presence of improper C-H···O hydrogen bonding. CH_2 scissoring deformations are expected to occur in the region 1465-1445 cm^{-1}[1,24]. The IR band at 1516 cm^{-1} and Raman band at 1474 cm^{-1} are assigned to the scissoring deformation modes of vibrations of CH_2-I and CH_2-II. CH_2 wagging deformations are expected to spread out over a wide wavenumber region 1382-1170 cm^{-1}[1,27]. This has been observed for CH_2-I as a strong band at 1324 cm^{-1} in IR and a weak band at 1380 cm^{-1} in Raman. CH_2-II wagging deformations are observed as medium band at 1273 cm^{-1} in IR and as weak band at 1260 cm^{-1}in Raman. CH_2 twisting deformations are expected over a region of wavenumbers 1295-1063 cm^{-1}[1,28]. The observed bands at 1353cm^{-1} in IR and 1351 cm^{-1} in Raman are assigned to CH_2-I twisting mode of vibration. The band at 1244cm^{-1} in IR is identified to CH_2-II twisting mode of vibration. CH_2 rocking deformations are expected to occur in the region 1174-724 cm^{-1}[1,28]. The IR band at 1030 cm^{-1} and Raman band

at 1040 cm^{-1} are assigned to the CH_2-II rocking mode of vibration. In addition, CH_2-Irocking modes are observed at 920 cm^{-1} in IR and at 922 cm^{-1} in Raman.

4.4.5 CH Vibrations

C-H stretching generally occurs in the region 3100-2800 cm^{-1}[1,22] and its deformation lies in the region at 1350-1315 cm^{-1}, respectively[27]. The observed strong band at 2853 cm^{-1} in IR and weak band at 2832 cm^{-1} in Raman are assigned to CH stretching mode of vibration. The band at 1444 cm^{-1} in IR is assigned to the rocking mode of vibration.

4.4.6 Carbonyl Group Vibrations

The carbonyl C=O stretching vibrations are expected to occur in the region 1760-1730 cm^{-1}[1,28]. The intense observed IR band at 1718 cm^{-1} is assigned to C=O stretching mode. When a carbonyl group participates in hydrogen bonding, resonance can occur, which puts a partial negative charge on the oxygen atom accepting the hydrogen bond and a positive charge on the atom donating the hydrogen and lowers the C=O stretching wavenumber. The shifting of the carbonyl stretching wavenumber is due to intramolecular charge transfer[29] and this indicates the NLO activity of LGO. The C-O stretching mode and O-H bending modes are not independent vibrational modes because they couple with the vibrations of adjacent groups. The carboxylic acid C-O stretching and O-H in plane bending modes are expected in the region 1440-1210 cm^{-1} [21]. The observed band at 1172 cm^{-1} in IR assigned to C-O stretching is coupled with O-H bending mode.

4.4.7 Carboxylate Vibrations

COO^- deformations are usually expected to occur in the region 650-510 cm^{-1}[1,30] and the rocking in-plane and out-of-plane deformation vibrations are observed in the region 760-400 cm^{-1}[1,31]. The bands at 721cm^{-1} in IR and at 715cm^{-1} in Raman are assigned to COO^- deformation mode, which is in good agreement with the theoretical value 722cm^{-1} and it may be responsible for the intermolecular charge transfer from a proton donor to a proton acceptor through the hydrogen bonds. The wagging modes of carboxylate vibrations have been identified at 805 cm^{-1} in IR.

4.4.8 Skeletal Mode Vibrations

The skeletal stretching vibrations of the amino acids are all coupled together. Of the skeletal vibrations, the C-C and C-N stretching modes lie in the region 1260-700 cm^{-1} and the deformation bands occur below 600 cm^{-1}[1,32]. The medium intensity bands at 1413, 1075 cm^{-1} in IR are assigned to CN stretching mode. The bands at 976, 870 and 747cm^{-1} in IR and at 968, 875 and 741 cm^{-1} in Raman are indicating the C-C stretching modes.

4.5 Hyperpolarizability Analysis

First-order hyperpolarizability β_{tot} and its related properties were calculated using B3LYP/6-311++G(d,p) level. The simultaneous occurrence of CH_2 asymmetric stretching modes of LGO (both in FTIR and FT-Raman) explains the charge transfer interaction which supports NLO activity. The hyperpolarizability was calculated by DFT/B3LYP/6-311++G(d,p) level based on the finite field approach theory are listed in Table 5. The title compound displays excellent first-order hyperpolarizability (β_{tot} = 1587.75x10^{-33}esu) and was 2 times the magnitude of urea.

4.6 Electronic Spectra Analysis

Molecular orbitals of LGO are shown in Figures 5 and 6. The predicted HOMO and LUMO energy values are -7.04eV and -1.21eV, respectively. The energy gap value is found to be 5.83eV. The decrease in the HOMO and LUMO energy gap explains the charge transfer interactions in the molecule and is responsible for the NLO activity of the molecule.

Table 5. Dipole moment, polarizability, hyperpolarizability components of LGO

Dipole moment (μ)		**Polarizability (α)**		**Hyperpolarizability (β)**	
Components	**value (Debye)**	**Components**	**value (a.u.)**	**Components**	**value (a.u)**
μ_x	0.96	α_{xx}	112.37	β_{xxx}	98.96
μ_y	-0.02	α_{xy}	-0.56	β_{yxx}	-41.63
μ_z	-0.85	α_{yy}	113.48	β_{xyy}	19.97
μ_{tot}	1.25	α_{xz}	-8.45	β_{yyy}	7.42
		α_{yz}	5.66	β_{zxx}	-98.92
		α_{zz}	154.01	β_{xyz}	189.78
		α_{tot}	18.76×10^{-24}e.s.u	β_{zyy}	178.21
				β_{xzz}	100.76
				β_{yzz}	418.22
				β_{zzz}	-4151.45
				β_{tot}	1587.75×10^{-33}e.s.u

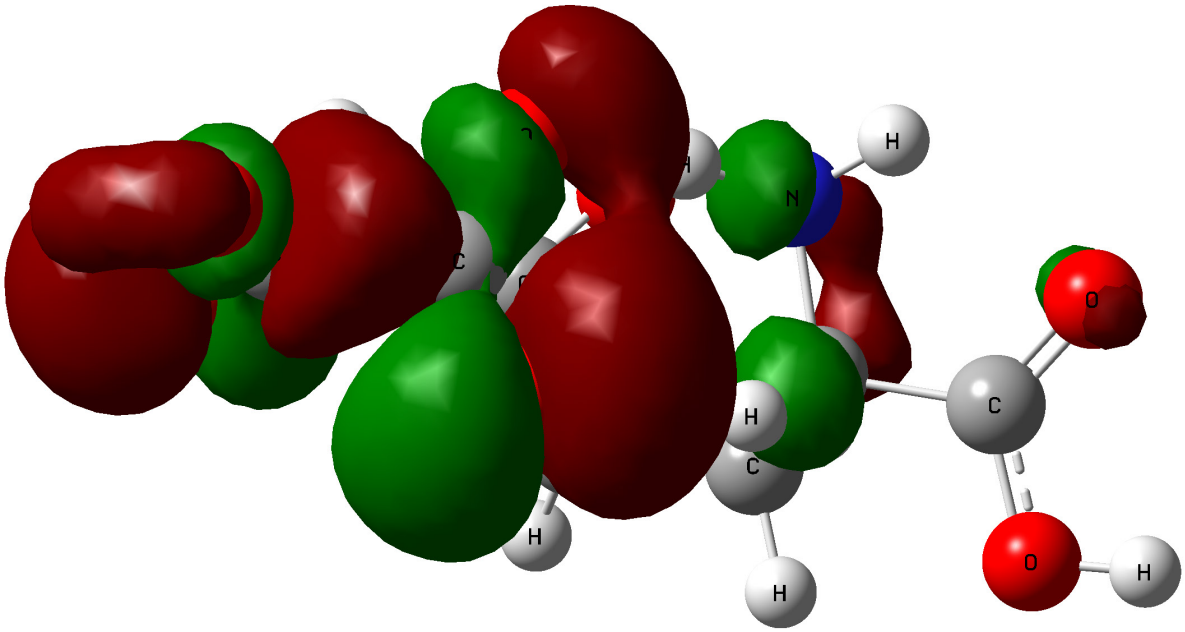

Figure 5. HOMO plot of LGO.

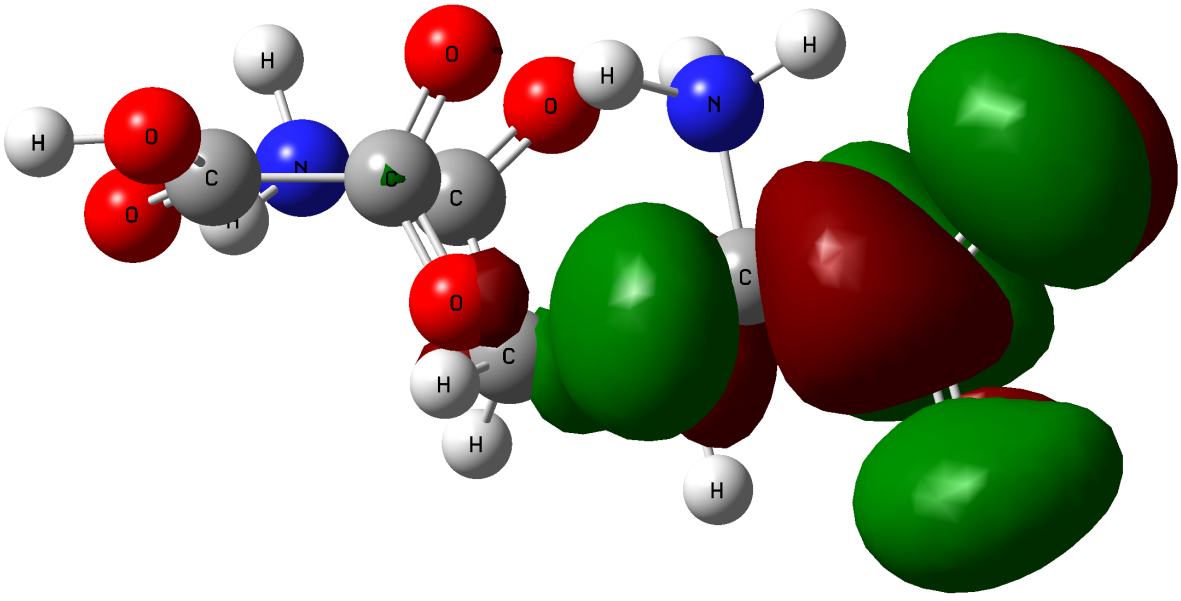

Figure 6. LUMO plot of LGO.

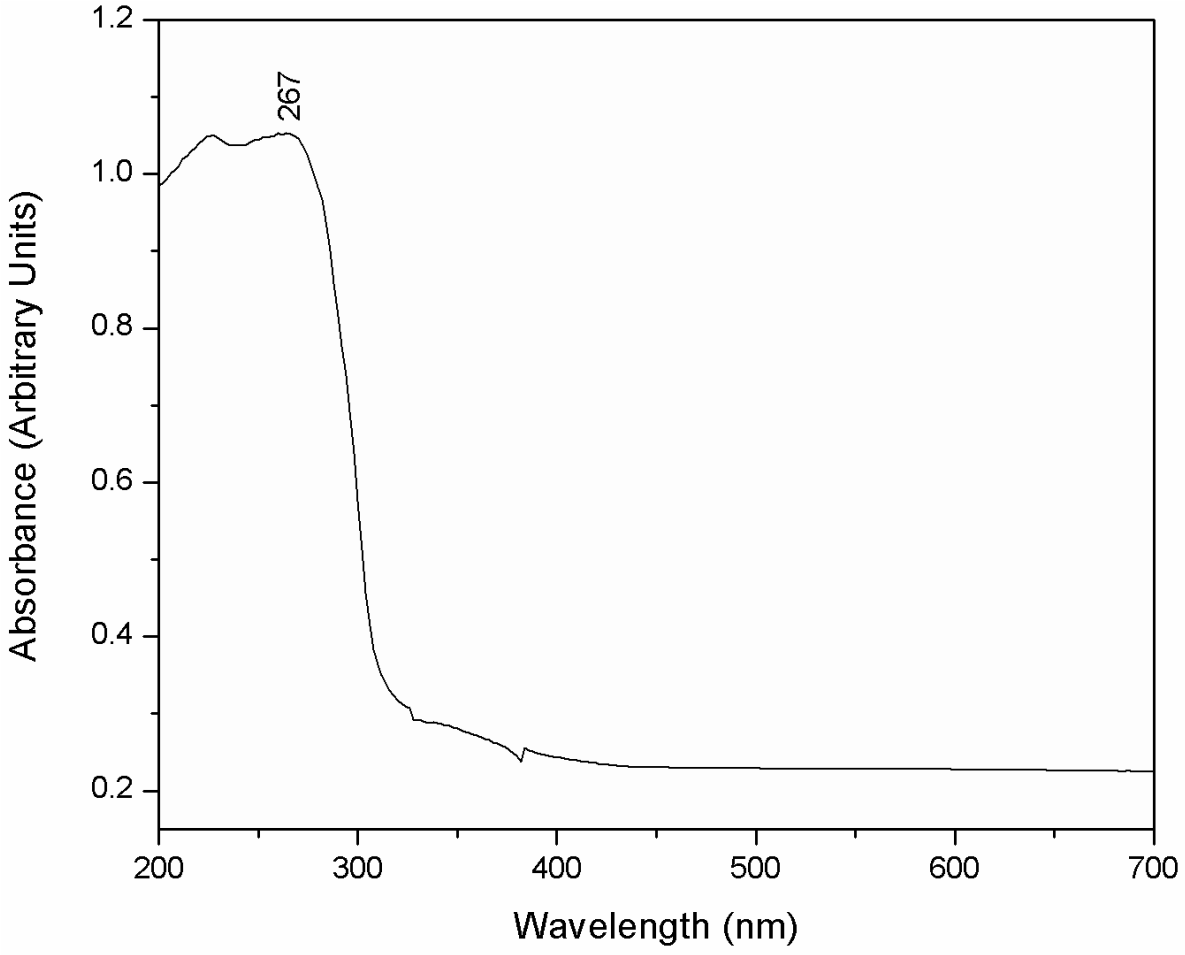

Figure 7. UV-Vis Absorption spectrum of LGO.

Nonlinearoptical material which has wide transparency window in the near IR, visible and in particular no absorption of light in the required wavelength, is used in many fields, so that the transmission spectrum is very important for any NLO material. The electronic UV-Vis absorption spectrum of LGO is shown in Figure 7. For LGO, the UV transparency cut-off occurs around 267 nm. High transmittance or low absorbance observed in the visible region with low cut-off wavelength confirms the suitability of LGO crystals for NLO applications. In order to understand electronic transitions, TD-DFT calculations on electronic absorption spectra analysis performed are tabulated in Table 6. In UV absorption spectrum peaks are observed at 267and 225 nm (Figure 7) while the calculated absorption maxima values are at 228, 218 and 214 nm. TD-DFT calculation predicts this excitation at 228 nm and this electronic absorption belongs to the transition from the ground to the first excited state mainly described by the one electron excitation from the HOMO to LUMO. Generally UV absorption band of amino acids

Table 6. Electronic excitation energy and oscillator strength of LGO calculated at B3LYP/6-311++G(d,p) level

No.	Experimental Wavelength (nm)	Energy (eV)	Calculated wavelength (nm)	Oscillator Strength (f)	Symmetry	Excited states
1.	267	5.43	228.25	0.0016	Singlet-A	HOMO→L+1 (83%)
2.	225	5.66	218.90	0.0018	Singlet-A	H-1→L+1 (10%), H-1→L+2 (69%)
3.		5.78	214.34	0.0065	Singlet-A	HOMO→LUMO (26%), HOMO→L+4 (13%), HOMO→L+5 (33%)

expected to occur in the region 200-280nm[33,34]. The absorption spectrum gives strong absorption band at 225 nm experimentally, and the corresponding theoretical peak at 228 nm is concerned with the HOMO→LUMO+1 electronic transitions which is assigned to $\pi \rightarrow \pi^*$ transition.

4.7 Molecular Electrostatic Potential Analysis

As it can be seen from the Figure 8, negative region is mainly localized over the oxygen atoms of the carbonyl group indicating a possible site for electrophilic attack. The maximum positive region is localized on the amino group with a value of +7.670e-2, indicating a possible site for nucleophilic attack. These sites give information about the region from where the compound can have intermolecular interactions. The positive potential shows the acceptor nature and the oxygen shows the negative potential or donor nature. This gives evidence for the possibility of N-H···O hydrogen bonding.

4.8 Mulliken Atomic Charge Population Analysis

The Mulliken atomic charges were calculated at the B3LYP/6-311++G(d,p) level of basis set. Figure 9 shows the Mulliken atomic net charges in LGO. The atom C_3 shows more negative charge (-0.687e) and atom H_{28} has more positive charge (0.52e) which suggests extensive charge delocalization in the molecule. The bonding capacity of a molecule depends on the electronic charge on the chelating atoms[35]. In LGO, the charges on C_1, C_2, C_3, C_5, C_{22}, C_{23} atoms are negative where as the remaining

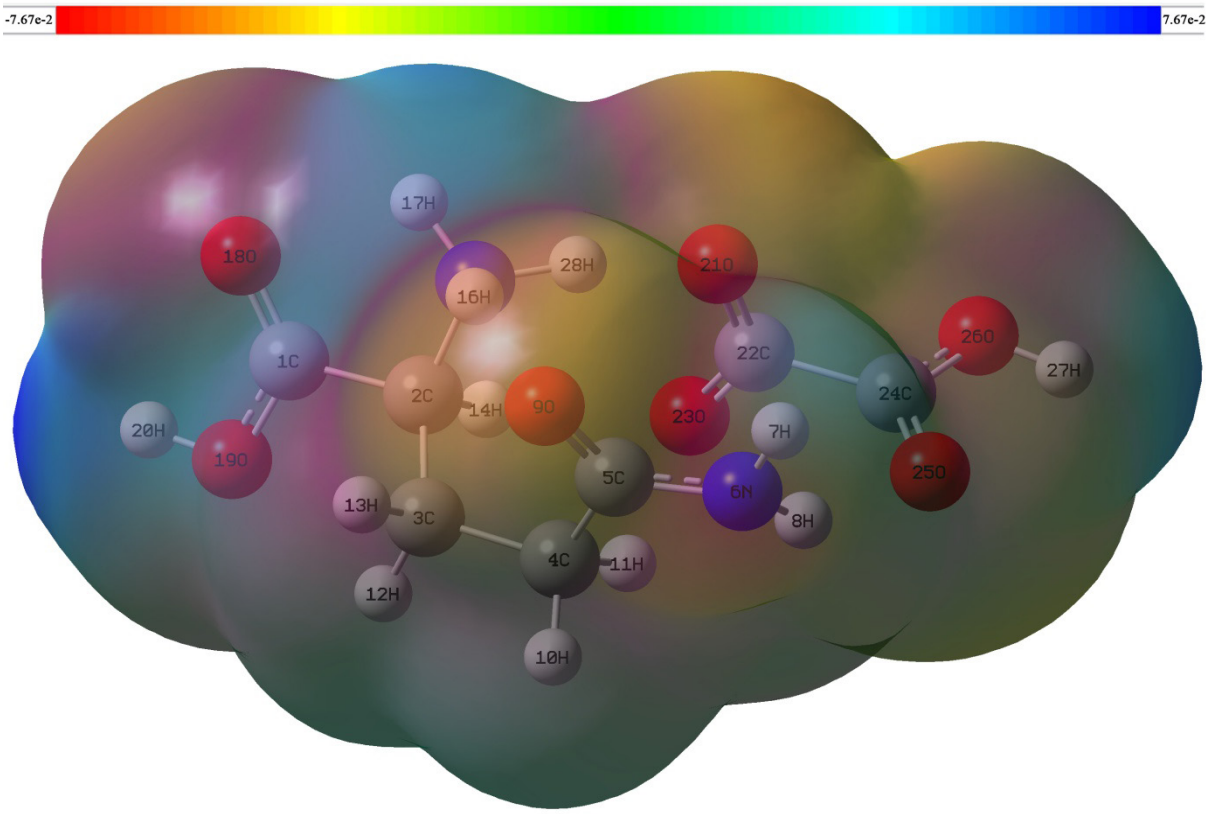

Figure 8. Molecular electrostatic potential of LGO.

carbons C_4, C_{24} are positively charged showing that C_{24} is bonded with electronegative oxygen atom. The shortening of bond length C_{24}= O_{25} supports this conclusion. The high electron density (1.9864e) of N_{15}-H_{28} leads to the increasing of its bond length and decreasing of its stretching wavenumber. The electron density is transferred from N_{15}-H_{28} to the antibonding σ*orbital of O_{21}-C_{22} bond, explaining both the elongation and the red-shift. This results support NBO analysis. All these results suggest that the atoms bonded to the hydrogen atoms and all oxygen atoms are electron acceptor.

4.9 Second Harmonic Generation Analysis

The Kurtz and Perry technique[36] was performed to analyse the second harmonic generation from LGO sample. A high density Nd:YAG laser (λ=1064 nm) with a pulse duration of 5ns was passed through the powdered sample of LGO. Second harmonic generation is confirmed by the emission of green radiation of wavelength 532 nm. The SHG efficiency of LGO was evaluated to be 0.27 times of urea. LGO crystal replicates good NLO property.

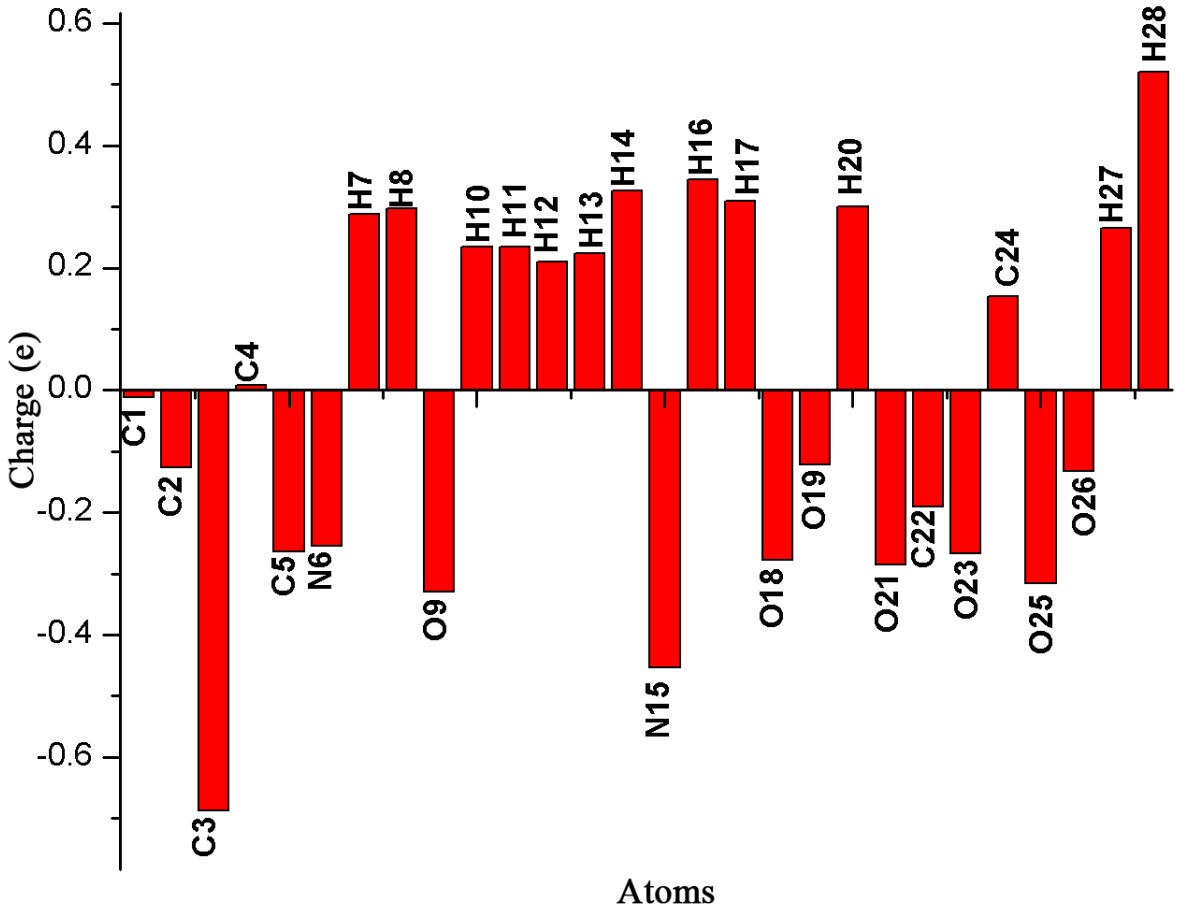

Figure 9. Mulliken charge distribution plot of LGO.

5. Conclusion

L-Glutamine oxalate crystals were grown by slow evaporation technique and characterized by powder XRD analysis. FTIR, FT-Raman spectra of LGO were recorded and analyzed. The assignments of the vibrational spectra has been carried out by normal coordinate analysis. The molecular geometry, HOMO and LUMO energy, vibrational wavenumbers of LGO has been evaluated by using DFT method. Red shifting of NH_3^+ stretching vibrations indicates the presence of N-H···O hydrogen bonding. Simultaneous occurrence of CH_2 asymmetric stretching mode explains the charge transfer interaction. There is excellent matching between the observed and the calculated wavenumbers. HOMO-LUMO energy gap value indicates the NLO activity of the molecule. The optical absorption spectral analysis supports that the crystals have low absorption with lower UV cut-off around 267 nm, showing the NLO property of crystals. The first-order hyperpolarizability value is two times of urea. Kurtz and Perry technique studies confirm the second order nonlinear optical properties of the molecule.

6. References

1. Ding YJ, Mu X, Gu X. Growth, Optical, Thermal and Di-electric Studies of an Amino Acid Organic Nonlinear Optical Material: l-Alanine. Journal of Nonlinear Optical Physics and Material. 2000; 9:21. Crossref.
2. Wang XQ, Xu D, Lu MK, Yuan DR, Xu SX. Crystal growth and characterization of the organometallic nonlinear optical crystal: manganese mercury thiocyanate (MMTC). Materials Research Bulletin. 2001; 36:879-87. Crossref.
3. Pawlukojc A, Hołderna-Natkaniec K, Bator G, Natkaniec I. L-glutamine: Dynamical properties investigation by means of INS, IR, RAMAN, 1 H NMR and DFT techniques. Journal of Chemical Physics. 2014; 443:17-25. Crossref.
4. Hanumantharao R, Kalainathan S. Studies on structural, thermal and optical properties of novel NLO crystal bis L-glutamine sodium nitrate. Materials Letters. 2012; 74:74-7. Crossref.
5. Qiushuo Yu, Xiaoxun Ma, Long Xu. Solubility, dissolution enthalpy and entropy of L-glutamine in mixed solvents of ethanol plus water and acetone plus water. Thermochimica Acta. 2013 April; 558:6-9. Crossref.
6. Amalanathan M, Hubert Joe I and Prabhu SS. Charge Transfer Interaction and Terahertz Studies of a Nonlinear Optical Material L-Glutamine Picrate: A DFT Study. The Journal of Physical Chemistry A. 2010; 114(50):13055-64. Crossref.PMid:21105650.
7. Frischet MJ et al. Wallingford CT: Gaussian, Inc.: Gaussian 09, Rev.A.02. 2009.
8. Becke AD. Density-functional thermochemistry III. The role of exact exchange. The Journal of Chemical Physics. 1993 April; 98(7):5648-52. Crossref.
9. Becke AD. Density-functional exchange-energy approximation with correct asymptotic behavior. Physical Review. 1988 September; A38:3098-100. Crossref.
10. Lee C, Yang W, Parr RG. Development of the Colle-Salvetti correlation-energy formula into a functional of the electron density. Physical Review. 1988; 378:785-9. Crossref.
11. Glendening ED, Reed AE, Carpenter JE, Weinhold F. NBO 3.1. Madison, WI: Theoretical Chemistry Institute, University of Wisconsin. 1998. PMCid:PMC21353.
12. Sundius T. Molvib - A flexible program for force field calculations. Journal of Molecular Structure. 1990; 218:321-6. Crossref.
13. Sundius T. Scaling of ab initio Force Fields by MOLVIB. Vibrational Spectroscopy. 2002; 29:89-95. Crossref.
14. Glendening ED, Reed AE, Carpenter JE, Weinhold F. NBO Version 3.1, TCI.
15. Madison: University of Wisconsin. 1998.
16. Reed AE, Curtiss LA, Weinhold F. Intermolecular interactions from a natural bond orbital, donor-acceptor viewpoint. Chemical Reviews. 1988; 88:899-926. Crossref.
17. Pulay P, Fogarasi G, Pang F, Boggs JE. Systematic ab initio Gradient Calculation of Molecular Geometries, Force Constants and Dipole Moment Derivatives. Journal of the American Chemical Society. 1979; 101:2550-60. Crossref.
18. Rauhut G, Pulay P. Transferable Scaling Factors for Density Functional Derived Vibrational Force Fields. Journal of Physical Chemistry. 1995; 99:3093-100. Crossref.
19. Socrates G. NewYork: Wiley: Infrared characteristic group frequencies. 1980. PMid:6937417.
20. Maroulis G. Electric multipole moment, dipole and quadrupole (hyper) polarizability derivatives for HF. Journal of Molecular Structure (Theochem). 2003; 633:177-97. Crossref.
21. Lin-Vien D, Colthup NB, Fateley WG, Grasellim JG. New York: Academic Press: The Hand Book of Infrared and Raman Characteristic Frequencies of Organic Molecules. 1991.
22. Bellamy LJ. NewYork: John Wiley and sons: The infrared spectra of complex Molecules. 1980. Crossref.
23. Silverstin RM, Webster FX. Newyork: Wiiley: Spectrometric Identification of organic compounds sixth ed. 1998.
24. Jesintha John C, Xavier TS, Amalanathan M, Hubert Joe I, Rastogi VK. Analysis of vibrational spectra and nonlinear optical properties of organic molecule l-alaninium formate. Spectrochimica Acta Part A. 2012; 86:174-80. Crossref. PMid:22074889.
25. Smith BC. New York: CRC Press: Infrared spectral interpretation: A systematic approach. 1999.
26. Snehalatha M, Ravikumar C, Sekar N, Jayakumar VS and Hubert Joe I. FT-Raman, IR and UV-visible spectral investigations and ab initio computations of a nonlinear food dye amaranth. Journal of Raman Spectroscopy. 2008; 39(7):928-36. Crossref.
27. Ravikumar C, Hubert Joe I, Jayakumar VS. Charge transfer interactions and nonlinear optical properties of push-pull chromophore benzaldehyde phenylhydrazone: A vibrational approach. Chemical Physics Letters. 2008; 460(4):552-8. Crossref.

28. Dollish FR, Fateley WG, Bentley FF. NewYork: Wiley: Characteristic Raman frequencies of organic compounds. 1973.
29. Colthup NB, Daly LH, Willely SE. NewYork: Academic Press: Introduction to infrared and Raman spectroscopy. 1990.
30. John Clarkson, Ewen Smith W. A DFT analysis of the vibrational spectra of nitrobenzene. Journal of Molecular Structure. 2003; 655:413-22. Crossref.
31. Dollish FR, Fateley WG, Bentley FF. New York: John Wiley and Sons: Characteristic Raman Frequencies of Organic Compounds. 1997.
32. Socrates G. England: John Wiley and Sons Ltd.: Infrared and Raman Characteristic Group Frequencies. 2001.
33. Mary MB, Umadevi M, Pandiarajan S, Ramakrishnan V. Vibrational spectral studies of l-methionine l-methionium perchlorate monohydrate. Spectrochimica Acta Part A. 2004; 60:2643-51. Crossref. PMid:15294255.
34. Layne E. Spectrophotometric and Turbidimetric Methods for Measuring Proteins. Methods in Enzymology. 1957; 3:447-55. Crossref.
35. Stoscheck CM. Quantitation of Protein. Methods in Enzymology. 1990; 182:50-68. Crossref.
36. Mulliken RS. Electronic population analysis on Lcao-Mo molecular wave functions. Journal of Chemical Physics. 1955; 23:1833-40. Crossref.
37. Kurtz SK, Perry TT. A Powder Technique for the Evaluation of Nonlinear Optical Materials. Journal of Applied Physics. 1968; 39(8):3798-813. Crossref.